HOKKAIDO UNIVERSITY

Title	Sema3A-and ascorbate-functionalized apatite-collagen scaffolds for enhanced bone regeneration
Author(s)	Banerjee, Kaushita; Ishii, Hanae; Oyane, Ayako et al.
Citation	MRS Communications, 15, 1105-1112 https://doi.org/10.1557/s43579-025-00796-9
Issue Date	2025-08-21
Doc URL	https://hdl.handle.net/2115/98040
Rights	This version of the article has been accepted for publication, after peer review (when applicable) and is subject to Springer Nature's AM terms of use, but is not the Version of Record and does not reflect post-acceptance improvements, or any corrections. The Version of Record is available online at: http://dx.doi.org/10.1557/s43579-025-00796-9
Type	journal article
File Information	ApAS-Sema Manuscript.pdf

Hokkaido University Collection of Scholarly and Academic Papers : HUSCAP

Sema3A- and ascorbate-functionalized apatite–collagen scaffolds for enhanced bone regeneration

Kaushita Banerjee[a, †], Hanae Ishii[b, †], Ayako Oyane[a, *], Maki Nakamura[a], Tomoya Inose[a], Erika Nishida[b], Kari Tsukita[b], Tomoka Hasegawa[c] and Hirofumi Miyaji[b, *]

[a]Research Institute of Core Technology for Materials Innovation, National Institute of Advanced Industrial Science and Technology (AIST), AIST Tsukuba Central 5, 1-1-1 Higashi, Tsukuba 305-8565, Japan.

[b]General Dentistry, Department of Oral Health Science, Faculty of Dental Medicine, Hokkaido University, N13W7, Kita-ku, Sapporo 060-8586, Japan

[c]Ultrastructure of Hard Tissue, Department of Oral Health Science, Faculty of Dental Medicine, Hokkaido University, N13W7, Kita-ku, Sapporo 060-8586, Japan

† These authors contributed equally to this work.

***Corresponding Authors**

Dr. Ayako Oyane,
Research Institute of Core Technology for Materials Innovation,
National Institute of Advanced Industrial Science and Technology (AIST),
E-mail: a-oyane@aist.go.jp, Phone: +81-50-3521-1018

Dr. Hirofumi Miyaji,
General Dentistry, Department of Oral Health Science, Faculty of Dental Medicine, Hokkaido University,
Email: miyaji@den.hokudai.ac.jp, Phone: +81-11-706-4312; +81-11-706-4221

Acknowledgments

The authors thank Ms. Miyabi Makino, Ms. Hiroko Araki, and Ms. Ikuko Sakamaki (AIST) for their technical support. This study was supported by Japan Society for the Promotion of Science (JSPS) KAKENHI, grant numbers JP23KF0095, JP22H05148, and JP22K10012.

Abstract

Porous collagen sponges coated with low-crystalline apatite are promising bone tissue regeneration scaffolds owing to their chemical similarity to natural bones. We previously fabricated an apatite-coated collagen sponge loaded with an osteogenic agent L-ascorbic acid 2-phosphate (AS), demonstrating its superior functionality. In the present study, this sponge was further functionalized with another osteogenic agent, semaphorin 3A (S3). The collagen sponge was first coated with AS-immobilized apatite by a biomimetic coating process using a supersaturated calcium phosphate solution, and then impregnated with S3 *via* drop-casting. The resulting sponge showed improved bone regeneration in a rat calvarial defect model *via* enhanced cell infiltration, angiogenesis, osteogenesis, and bone remodeling, while being resorbed by macrophage-mediated processes, highlighting its potential as a bone tissue regeneration scaffold.

Keywords: composite, coating, solution deposition, biomimetic, bone, biomaterial

Introduction

Despite the bone's intrinsic capacity for self-repair, its regenerative potential is insufficient to repair critically sized defects.[1,2] Autologous bone is the gold standard for bone tissue regeneration because of its strong osteogenic properties; however, it is limited by donor site morbidity and supply limitations.[3-5]

Various synthetic scaffolds using biocompatible, bioresorbable, and osteoconductive materials have been developed for bone tissue regeneration.[1-5] Among them, apatite-coated collagen sponges are notable for their chemical similarity to natural bone.[6-10] We previously developed a 3D porous collagen sponge coated with low-crystalline apatite using a plasma- and precursor-assisted biomimetic coating process, showing superior bone regeneration and resorption properties to the uncoated sponge.[7,8] More recently, we immobilized the osteogenic agent L-ascorbic acid 2-phosphate (AS) in the apatite coating on the collagen sponge *via* a modified coating process.[10] The resulting collagen sponge with AS-immobilized apatite coating (**ApAS**) exhibited better cytocompatibility with osteoblastic cells than the apatite-coated collagen sponge. **ApAS** is anticipated to function even better as a bone regeneration scaffold by incorporating another osteogenic agent, semaphorin 3A also known as Sema3A (S3). Combining AS and S3 may enhance bone regeneration, as AS stimulates osteoblast differentiation and matrix mineralization by functioning as an enzyme cofactor essential for collagen biosynthesis,[11,12] whereas S3 promotes osteoblastic bone formation and suppresses RANKL-mediated osteoclastic bone resorption, regulating the bone remodeling process.[13,14]

In this study, we fabricated **ApAS** by following our previous coating process using a metastable supersaturated calcium phosphate (CaP) solution supplemented with AS.[10] This study aims to develop and evaluate a dual-agent scaffold, **ApAS-S3**—created by incorporating S3 into **ApAS**—for its *in vivo* bone regeneration efficacy using a rat calvarial defect model.

Materials and Methods

Scaffold preparation

The untreated collagen sponge *viz.,* **Col**, was prepared by cutting a 3D porous atelocollagen sponge sheet (Terudermis; GC Corporation, Tokyo, Japan) into circular discs with diameters of 5 mm. To prepare **ApAS**, **Col** was subjected to plasma- and precursor-assisted biomimetic coating using an AS-supplemented CaP solution as previously reported.[10] Before coating, a metastable supersaturated CaP solution (NaCl 142 mM, $K_2HPO_4 \cdot 3H_2O$ 1.5 mM, $CaCl_2$ 3.75 mM, buffered to pH 7.40 at 25 °C with 50 mM of tris(hydroxymethyl)aminomethane and HCl) was supplemented with 60 μg/mL L-ascorbic acid phosphate magnesium salt n-hydrate (AS source) (FUJIFILM Wako Pure Chemical Corporation, Osaka, Japan, Lot. WTF5181; n = 4.4; water content = 21.5 mass%). **Col** sponges were treated with oxygen plasma (0.1 W/cm²) for 2 min in a 30 Pa O_2 atmosphere using a compact ion etcher (FA-1, SAMCO Inc., Kyoto, Japan). Plasma-treated sponges were precoated with CaP *via* alternate immersion in 10 mL of 200 mM $CaCl_2$ and 200 mM $K_2HPO_4 \cdot 3H_2O$ aqueous solutions (for 20 min each) under reduced pressure (washed intermediately with ultrapure water). The CaP-precoated sponge was immersed in 10 mL of AS-supplemented CaP solution after prewashing with the same solution and was subsequently incubated at 25 °C for 24 h under orbital shaking at 150 rpm. Post incubation, the sponges were washed with ultrapure water and frozen at −80 °C, followed by lyophilization. Lyophilized sponges are referred to as **ApAS**.

Physiochemical analyses

The outer and inner surfaces of **Col** and **ApAS** were analyzed using a tabletop scanning electron microscope

(SEM; TM4000Plus II, Hitachi High-Tech Corporation, Tokyo, Japan) integrated with an energy-dispersive X-ray spectroscopy (EDX) system (AZtecOne, Oxford Instruments Plc, Abingdon, UK). The inner surface of sponges were exposed *via* bisection using a microtome blade (Feather S35; Feather Safety Razor Co., Ltd., Osaka, Japan). EDX measurements were performed without applying a conductive coating, whereas SEM imaging was conducted after gold sputter-coating using a sputtering device (SC-701MkII, Sanyu Electron Co., Ltd., Akishima, Japan).

To evaluate the crystalline structures, the outer surfaces of **Col** and **ApAS** were analyzed using an X-ray diffractometer (XRD; MiniFlex600-C, Rigaku Corporation, Tokyo, Japan). XRD measurements were performed *via* CuKα radiation at 40 kV and 15 mA, with a 2θ step size of 0.01° and a scan rate of 4°/min.

S3 incorporation into scaffold

Prior to implantation, **ApAS** sponges were impregnated with S3 *via* drop-casting to prepare **ApAS-S3**. Recombinant human semaphorin 3A Fc chimera protein (S3 source) (1250-S3-025; R&D Systems, Minneapolis, MN, USA) was reconstituted in phosphate-buffered saline (PBS (–); FUJIFILM Wako Pure Chemical Corporation) to obtain a working solution of 4 μg/mL S3. The working solution (50 μL) was drop-casted onto each **ApAS** sponge, aiming for a final S3 dose of 200 ng per sponge. This S3 dose was determined based on a previous result that incorporation of S3 (200 ng) into a scaffold was effective in enhancing reparative dentin formation in rats. [15]

The same volume (50 μL) of PBS without S3 was drop-casted onto each sponge of **Col** and **ApAS** before implantation.

Implantation in experimental rat calvarial defects

In vivo experiments using 10 week-old male Wistar rats (approximately 200 g) were conducted in accordance with the Institutional Animal Use and Care Regulations of Hokkaido University after obtaining approval from the University's Animal Research Committee (approval number: 24-114). Surgical procedures were performed under general anesthesia, induced *via* intraperitoneal medetomidine hydrochloride (0.15 μg/kg; Domitor, Nippon Zenyaku Kogyo Co., Ltd., Koriyama, Japan), midazolam (2.0 μg/kg; Dormicum, Astellas Pharma Inc., Tokyo, Japan), and butorphanol tartrate (2.5 μg/kg; Vetorphale, Meiji Seika Pharma Co., Ltd., Tokyo, Japan) administration, combined with a local injection of 2 % lidocaine hydrochloride with 1:80,000 epinephrine (Xylocaine Cartridge for Dental Use, Dentsply Sirona K.K., Tokyo, Japan). After elevation of the skin-periosteal flap, a 5.0 mm diameter critical-sized defect was created in the cranial bone of rats using a trephine bur (Meis Trephine Bur, Hager & Meisinger GmbH, Neuss, Germany) operated at ≤1,500 rpm under continuous sterile saline irrigation. Sponges of **Col**, **ApAS**, or **ApAS-S3** were implanted into calvarial defects. The skin was sutured (BioFit-D 4-0, Washiesu Medical Corp., Tokyo, Japan) post-surgery, and the wound was topically treated with Nadifloxactin ointment (Acuatim ointment 1 %, Otsuka Pharmaceutical Co., Ltd. Tokyo, Japan) to prevent postoperative infections.

X-ray microcomputed tomography analyses

Four weeks post-surgery, rats were euthanized *via* sodium pentobarbital (2.0 mL/kg, Pentobarbital Sodium Salt, NACALAI TESQUE, INC., Kyoto, Japan) administration, followed by transcardiac perfusion with 10 % formalin (Mildform 10 N; Fujifilm Wako Pure Chemical Corp.). Harvested calvarial bones were scanned using an X-ray microcomputed tomography (μCT) system (R_mCT2, Rigaku Corporation) to observe bone formation in the defect. The radiolucent (non-regenerated) and radiopaque (regenerated)

regions were quantified from μCT images, using image analysis software (ImageJ ver. 1.41; National Institutes of Health, Bethesda, MD, USA).

Histological and histomorphometric analyses

The extracted cranial bones were fixed in 10% buffered formalin, decalcified in 10% ethylenediaminetetraacetic acid (Fujifilm Wako Pure Chemical Corp.), embedded in paraffin, and sliced. Tissue sections were stained with hematoxylin–eosin (HE) and Masson's trichrome (MT). Tissue sections were observed under a light microscope (NanoZoomer S210 C13239-01; Hamamatsu Photonics K.K., Hamamatsu, Japan), and the area and length of the newly formed bone were measured using the image analysis software. Total number of cells and the number of multinucleated giant cells in the area of 200 μm × 500 μm were also measured by the method reported in a previous report [16].

Immunohistochemical analyses

The tissue sections were subjected to tartrate-resistant acid phosphatase (TRAP) staining using a TRAP/ALP stain kit (Fujifilm Wako Pure Chemical Corp.) according to the manufacturer's instructions. Specific antibodies were used to detect CD31, CD204, osteocalcin (OCN), and SP7. After thermal epitope retrieval, sections were incubated overnight with the following primary antibodies: rabbit anti-CD31 (1:2000; Abcam, Cambridge, UK), mouse anti-CD204 (1:200; Cosmo Bio, Tokyo, Japan), rabbit anti-OCN (1:400; Bioss, Woburn, MA, USA), and rabbit anti-SP7 (1:3000; Abcam). Secondary staining was performed with an appropriate secondary antibody, anti-mouse IgG or anti-rabbit IgG labeled with peroxidase (Histofine Simple Stain Rat MAX PO(MULTI), NICHIREI BIOSCIENCES INC., Tokyo, Japan). The antigen-antibody reaction sites were visualized using diaminobenzidine, and the stained

sections were observed using the optical microscope (NanoZoomer S210). Total number of cells and the number of positive cells in the area of 200 μm × 500 μm were measured to calculate the percent positive cells according to the previously reported method.[17]

Statistical analyses

For quantitative data, mean and standard deviation (SD) were calculated. Statistical differences were analyzed using one-way analysis of variance with Tukey's HSD post-hoc test (SPSS 11.0, IBM Corporation, Armonk, NY, USA). Differences with $p < 0.05$ were considered statistically significant.

Results and Discussion

Physiochemical analyses

We fabricated **ApAS**, *i.e.*, the collagen scaffold coated with AS-immobilized apatite, *via* our plasma- and precursor-assisted biomimetic coating process, as previously reported.[10] The presence of the coating on the porous collagen sponge was confirmed *via* physicochemical analyses. The SEM images (Fig. 1a) revealed particulate precipitates on both the outer and inner **ApAS** surfaces, different from the smooth surface of **Col**. These precipitates on **ApAS** were composed of CaP, as corroborated using EDX analyses (Fig. 1b). Before coating, **Col** showed C and O peaks, the main components of collagen, on both the outer and inner surfaces. A small amount of NaCl was also present on the **Col** surface as an accessory component. After coating, C peak intensity decreased, whereas Ca and P peaks appeared on both the outer and inner **ApAS** surfaces, suggesting CaP precipitation during coating. CaP precipitates on **ApAS** were identified as low-crystalline apatite using XRD; **Col** showed diffraction peaks attributed to NaCl, whereas **ApAS**

showed broad peaks corresponding to hydroxyapatite (Fig. 1c). These findings were consistent with those of our previous study.[10] According to this study, the AS content immobilized in **ApAS** was 201 ± 9 µg (per sponge).

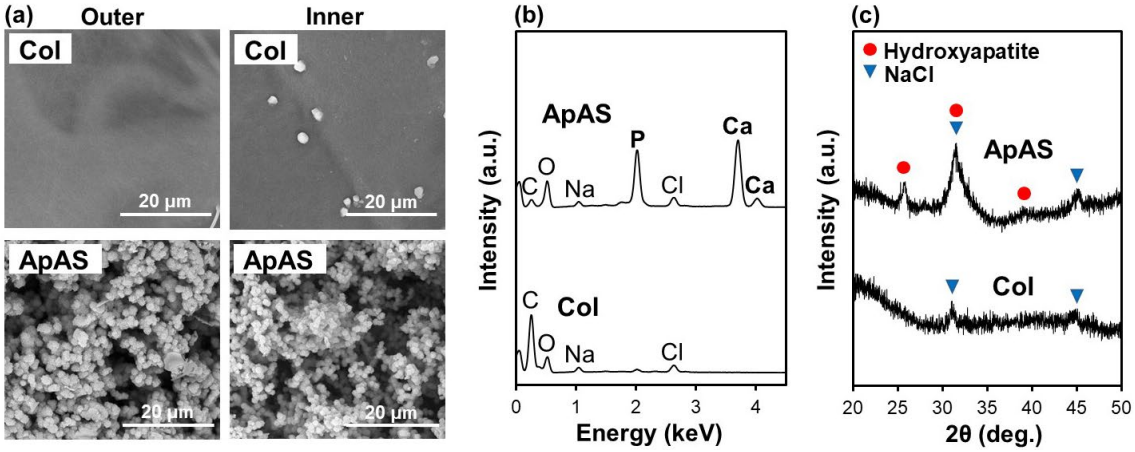

Fig. 1 (a) SEM images, (b) EDX spectra, and (c) XRD patterns of the outer and inner (only for (a)) surfaces of **Col** and **ApAS**.

µCT analyses

The regenerative potential of the scaffolds was assessed *via* implantation into calvarial bone defects in rats. Two rats (one each from the **Col** and **ApAS** groups) died during decortication, resulting in final group sizes of 5, 5, and 6 rats for the **Col**, **ApAS**, and **ApAS-S3** groups, respectively.

*µ*CT analyses showed that **ApAS-S3** aided in augmented bone tissue regeneration. Fig. 2a shows the representative *µ*CT images of the calvarial bones after implantation of **Col**, **ApAS**, and **ApAS-S3** in the critical-sized defect. **ApAS-S3** induced substantial bone regeneration (radiopaque regions indicated by yellow arrows) at the defect site. In contrast, **Col** and **ApAS** showed minimal bone regeneration, with defects hardly repaired (circular radiolucent region). Quantitative assessment revealed that the bone volume–to–total volume (BV/TV) fractions were 16 ± 11, 22 ± 10, and 41 ± 16 % for the **Col**, **ApAS**, and

ApAS-S3 groups, respectively, depicting a significantly (p <0.05) higher BV/TV fraction in **ApAS-S3** than in **Col** (Fig. 2b). **ApAS** exhibited an intermediate BV/TV fraction between **Col** and **ApAS-S3**; however, the difference with either **Col** or **ApAS-S3** was not statistically significant (p >0.05).

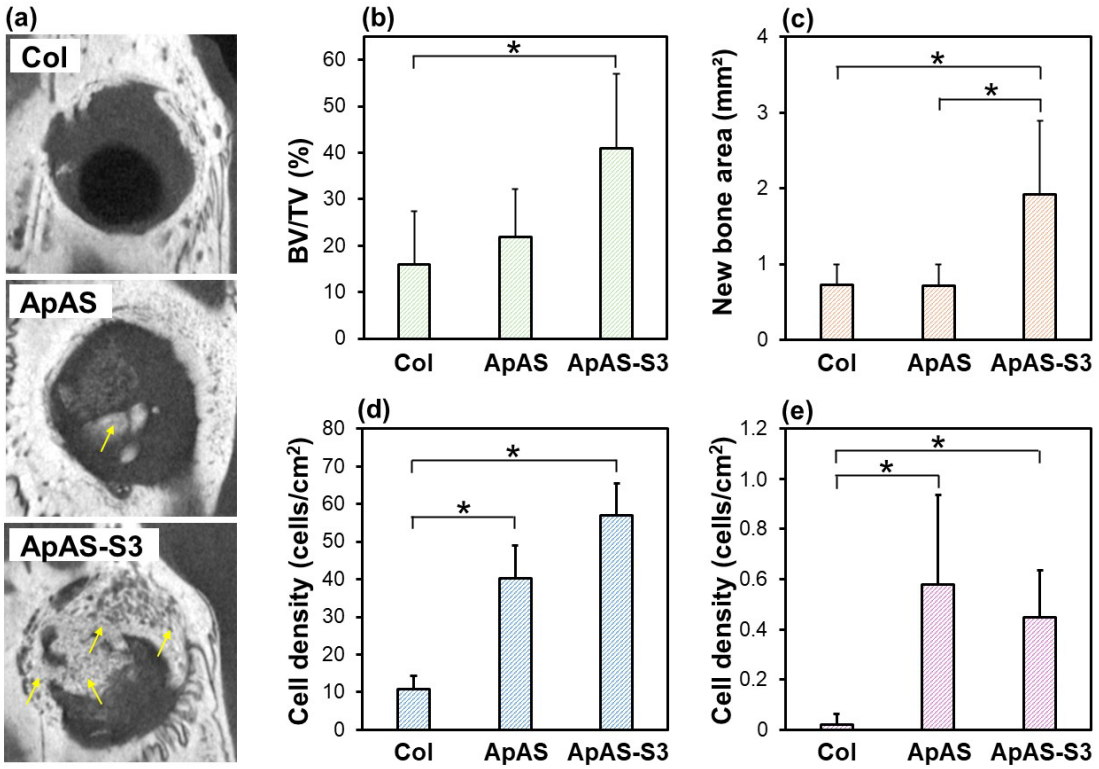

Fig. 2 (a) μCT images, (b) bone volume–to–total volume (BV/TV) fraction (from μCT images), (c) area of the newly formed bone tissue (from histological images), and density of (d) total and (e) giant cells (from histological images), of the calvarial bone defects after **Col**, **ApAS**, and **ApAS-S3** implantation (n = 6 for **ApAS-S3** and n = 5 for **Col** and **ApAS**; mean + SD, *p <0.05). Yellow arrows in (a) indicate the radiopaque regenerated regions.

Histological and histomorphometric analyses

Histological evaluation confirmed that **ApAS-S3** enhanced bone tissue regeneration. Fig. 3a (right) shows abundant newly formed bone (denoted by NB) at the defect site in the **ApAS-S3** group. In contrast, **Col**

(Fig. 3a, left) and **ApAS** (Fig. 3a, middle) induced limited bone regeneration. The residual scaffold (denoted by RS) and newly formed collagen fiber (distinguished by the differences in their structures and stainability) were observed at the defect sites in all groups (Fig. 3a,c). In the **ApAS** and **ApAS-S3** groups, more cells were found within the residual scaffold compared to those in the **Col** group, suggesting enhanced cell infiltration owing to the coating on **ApAS** and **ApAS-S3**, as reported for similar scaffolds.[6-8, 18] Histomorphometric measurements revealed significantly more newly formed bone in the **ApAS-S3** group than that in the **Col** and **ApAS** groups (Fig. 2c), corroborating histological observations. However, the difference between the **Col** and **ApAS** groups was not statistically significant. At higher magnification (Fig. 3b,d), **ApAS** and **ApAS-S3** revealed more fibroblastic and multinucleated giant cells (denoted by green arrows) than **Col**, likely associated with coating degradation on the mineralized sponges. Measurement of cell numbers revealed significantly higher densities of total cells (Fig. 2d) and multinucleated giant cells (Fig. 2e) within the residual scaffold in the **ApAS** and **ApAS-S3** groups compared to those in the **Col** group.

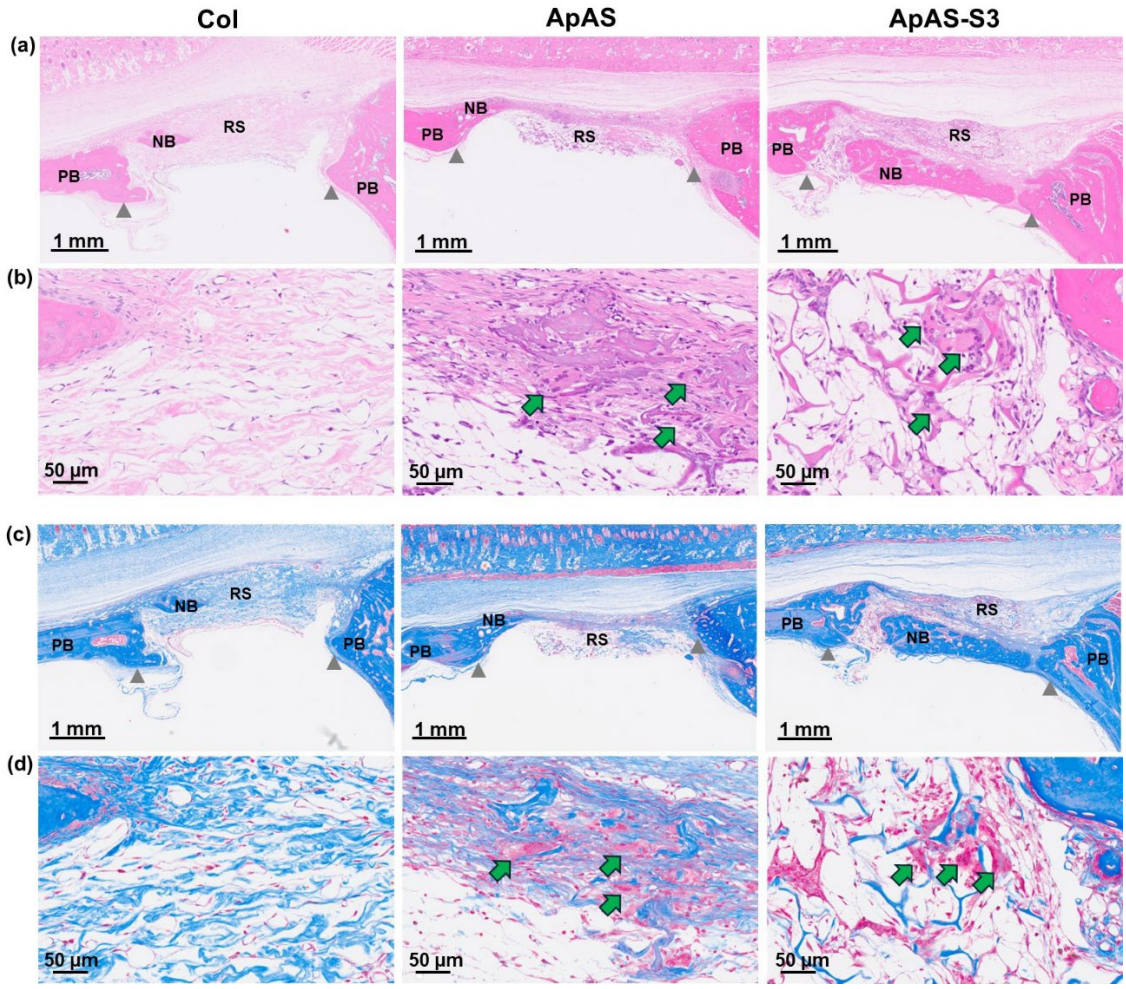

Fig. 3 Microscopic images, in (a,c) lower and (b,d) higher (regions surrounding newly formed bone) magnification, of the (a,b) HE- and (c,d) MT-stained histological sections prepared from calvarial bones after **Col** (left), **ApAS** (center), and **ApAS-S3** (right) implantation into the defect. (a,c) Gray arrowheads: borders of the initial defect, NB: New bone, PB: Pre-existing bone, RS: Residual scaffold, (b,d) Green arrows: giant cells

Immunohistochemical analyses

Fig. 4 and Table 1 shows immunohistochemical analytical results of the **Col** , **ApAS**, and **ApAS-S3** groups. The **ApAS** and **ApAS-S3** groups showed a marked increase in CD31-positive cells, suggesting enhanced microvessel formation. This result indicates that the mineralized sponges induced angiogenesis, enabling a

sufficient supply of nutrients and oxygen, both of which are essential for tissue regeneration. A large number of CD204-positive macrophages were observed in the **ApAS** and **ApAS-S3** group, suggesting M2 macrophage-mediated tissue remodeling. Some of these macrophages were also TRAP-positive, implying their involvement in the dissolution of the apatite component of the mineralized sponges. In the **ApAS** and **ApAS-S3** group, TRAP-positive cells (ascribed to osteoclast, evident in the upper region) as well as OCN-positive and SP7-positive cells (ascribed to osteoblasts, evident in the lower region) were more prominent than in the **Col** group. This suggests that the mineralized sponges simultaneously induced active bone formation and remodeling. Therefore, the mineralized sponges (both **ApAS** and **ApAS-S3**) likely facilitated a sequence of angiogenesis, osteogenesis, and bone remodeling, leading to enhanced bone regeneration.

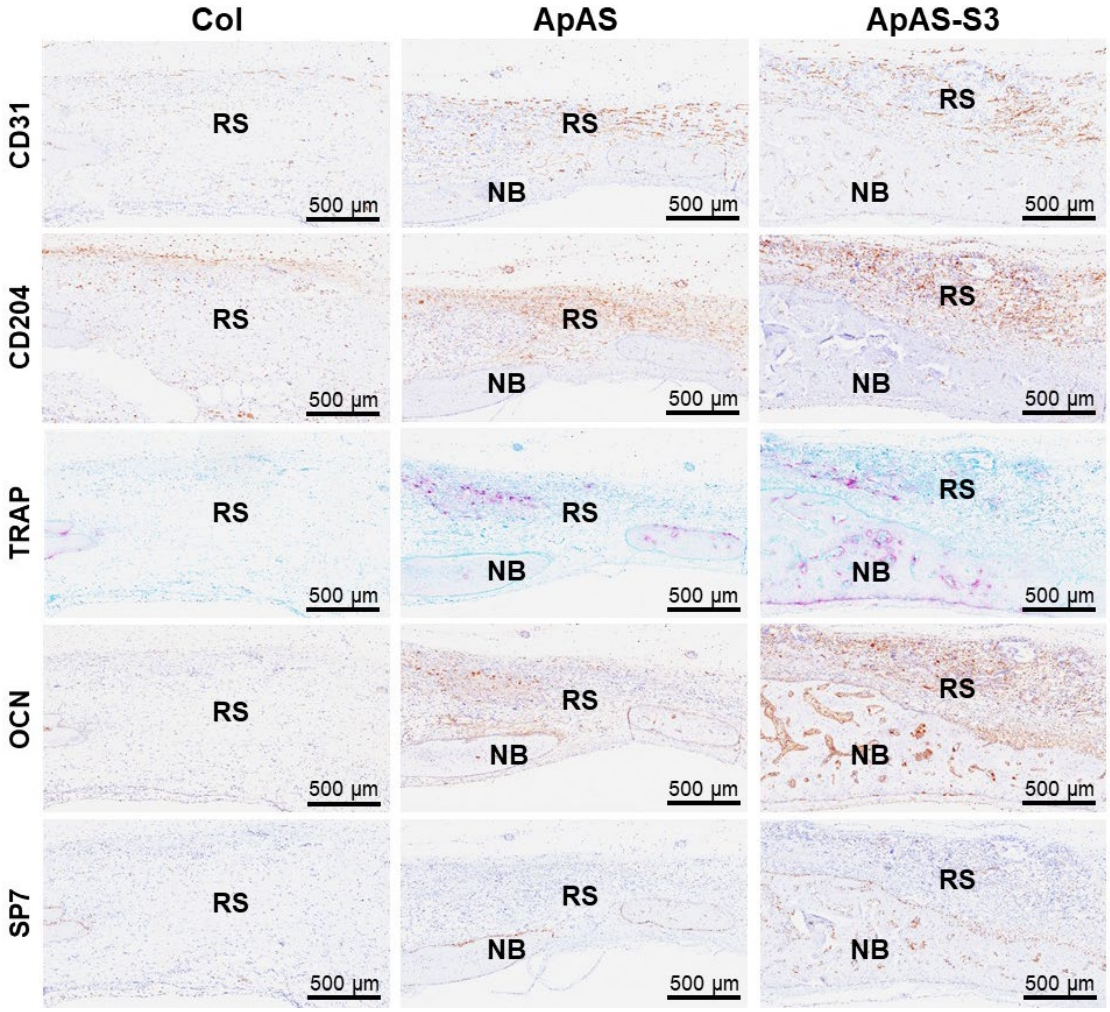

Fig. 4 Microscopic images of the CD31-, CD204-, TRAP-, OCN-, and SP7-stained histological sections prepared from calvarial bones after **Col** (left), **ApAS** (center), and **ApAS-S3** (right) implantation into the defect. NB: New bone, RS: Residual scaffold.

Table 1 Summary table of the immunohistochemical analytical results in Fig. 4 (except for TRAP-staining results).

	CD31	CD204	OCN	SP7
Col	+/–	+/–	–	–
ApAS	+	++	+	+
ApAS-S3	+	+	+	+

Signs of –, +/–, +, and ++ represent the percent positive cells (PPC) of PPC=0, 0<PPC<10, 10≤PPC≤50, and 50<PPC≤100, respectively.

Putative mechanism of action

As demonstrated in this *in vivo* study, **ApAS-S3** has potential as a scaffold for bone tissue regeneration. The putative mechanisms of action are as follows: The framework of **ApAS-S3** is a 3D porous collagen sponge coated with low-crystalline apatite. The 3D porous structure of the sponge is retained even after coating,[19] ensuring cell infiltration and vascularization inside the sponge, essential for 3D bone-tissue regeneration. The mineralized coating enhances infiltration of macrophages, osteoblasts, and osteoclasts, creating an osteogenic environment within the sponge.[7,20] AS, a stable derivative of vitamin C released from the mineralized coating, enhances bone tissue regeneration by facilitating osteoblast proliferation and differentiation[11,12,21] and collagen synthesis and crosslinking, essential for matrix maturation.[22] S3, a potent osteoprotective factor released from the mineralized sponge, modulates both osteoblast and osteoclast activity and stimulates osteoblast differentiation and bone matrix production.[13,14,23,24] Simultaneously, the mineralized sponge is resorbed by macrophage-mediated processes and replaced by regenerated bone tissue. Consequently, the prepared scaffold **ApAS-S3** showed superior bone-regenerative

capacity.

Limitations

This study is preliminary and has several limitations. First, release kinetics of both AS and S3 are yet to be clarified. Because S3 was immobilized on the mineralized sponge *via* drop-casting, the physically adsorbed S3 may show faster (possibly burst) release than AS that was immobilized in the apatite coating. Second, the current study design does not fully isolate the individual effects of S3 and AS. To elucidate the individual and potential synergistic effects of S3 and AS, another sample group, *i.e.*, an apatite-coated sponge loaded with only S3 (AS-free sponge) is required. Third, *in vivo* analysis was performed at a limited time point (4 weeks only) using a limited number of animals. Further *in vitro* and *in vivo* studies are needed to prove the clinical potential of **ApAS-S3** as a scaffold for bone tissue regeneration.

Conclusion

The addition of S3 to the AS-immobilized, mineralized collagen sponge (**ApAS**) improved bone regeneration in a rat calvarial defect model. Histological and immunohistochemical analyses revealed that **ApAS-S3** enhanced bone regeneration by facilitating cell infiltration, angiogenesis, osteogenesis, and bone remodeling, while being resorbed by macrophage-mediated processes. These results demonstrate the potential of **ApAS-S3** as a scaffold for bone tissue regeneration.

Acknowledgments

The authors thank Ms. Miyabi Makino, Ms. Hiroko Araki, and Ms. Ikuko Sakamaki (AIST) for their technical support.

Author contributions

Kaushita Banerjee: Methodology, Investigation, Formal analysis, Data Curation, Funding acquisition, Writing–Original Draft. Hane Ishii: Methodology, Investigation, Formal analysis, Data Curation, Writing–Original Draft. Ayako Oyane: Conceptualization, Methodology, Data Curation, Funding acquisition, Supervision, Project administration, Writing– Review & Editing. Maki Nakamura: Methodology, Supervision, Visualization, Writing–Review & Editing. Tomoya Inose: Investigation, Data Curation, Writing–Review & Editing. Erika Nishida: Investigation, Formal analysis, Data Curation, Funding acquisition, Writing–Review & Editing. Kari Tsukita: Investigation, Formal analysis,
Data Curation, Writing–Review & Editing. Tomoka Hasegawa: Methodology, Investigation, Writing–Review & Editing. Hirofumi Miyaji: Conceptualization, Methodology, Data Curation, Resources, Writing–Review & Editing.

Funding

This study was supported by Japan Society for the Promotion of Science (JSPS) KAKENHI, grant numbers JP23KF0095, JP22H05148, and JP22K10012.

Data availability

Data will be made available on reasonable request.

Declarations

Conflict of interest

The authors declare no conflict of interest.

References

1. Y. Zhao, Q. Wu, C. Zhao, H. Zhou, L. Wu, Compos. Struct. **349**–**350**, 118542 (2024). https://doi.org/10.1016/j.compstruct.2024.118542
2. A. Santoro, A. Voto, L. Fortino, R. Guida, C. Laudisio, M. Cillo, A.M. D'Ursi, Int. J. Mol. Sci. **26**, 3085 (2025). https://doi.org/10.3390/ijms26073085
3. R. De Pace, S. Molinari, E. Mazzoni, G. Perale, J. Clin. Med. **14**, 1838 (2025). https://doi.org/10.3390/jcm14061838
4. M.A. Schallenberger, K. Rossmeier, H.M. Lovick, T.R. Meyer, H.M. Aberman, G.A. Juda, J. Craniofac. Surg. **25**, 657–661 (2014). https://doi.org/10.1097/SCS.0000000000000610
5. H. Qu, H. Fu, Z. Han, Y. Sun, RSC Adv. **9**, 26252–26262 (2019). https://doi.org/10.1039/C9RA05214C
6. S. Santhakumar, A. Oyane, M. Nakamura, Y. Yoshino, M.K. Alruwaili, H. Miyaji, Materials **14**, 5860 (2021). https://doi.org/10.3390/ma14195860
7. A.J. Nathanael, A. Oyane, M. Nakamura, I. Sakamaki, E. Nishida, Y. Kanemoto, H. Miyaji, ACS Appl. Mater. Interfaces **9**, 22185–22194 (2017). https://doi.org/10.1021/acsami.7b04776
8. Y. Kanemoto, H. Miyaji, E. Nishida, S. Miyata, K. Mayumi, Y. Yoshino, A. Kato, T. Sugaya, T. Akasaka, A.J. Nathanael, S. Santhakumar, J. Periodont. Res. **57**, 205–218 (2022). https://doi.org/10.1111/jre.12954
9. X. Zhao, H. Li, Z. Xu, K. Li, S. Cao, G. Jiang, Surf. Coat. Technol. **322**, 227–237 (2017). https://doi.org/10.1016/j.surfcoat.2017.05.042
10. K. Banerjee, A. Oyane, M. Nakamura, T. Inose, E. Nishida, K. Shitomi, H. Miyaji, RSC Adv., **15,** 19480–19488 (2025). https://doi.org/10.1039/d5ra02963e
11. S. Takamizawa, Y. Maehata, K. Imai, H. Senoo, S. Sato, and R.I. Hata, Cell Biol. Int. **28**, 255–265 (2004). https://doi.org/10.1016/j.cellbi.2004.01.010
12. K. Tsutsumi, H. Fujikawa, T. Kajikawa, M. Takedachi, T. Yamamoto, S. Murakami, J. Period. Res. **47**, 263–271 (2012). https://doi.org/10.1111/j.1600-0765.2011.01430.x.
13. M. Hayashi, T. Nakashima, M. Taniguchi, T. Kodama, A. Kumanogoh, H. Takayanagi, Nature **485**, 69–74 (2012). https://doi.org/10.1038/nature11000
14. T. Fukuda, S. Takeda, R. Xu, H. Ochi, S. Sunamura, T. Sato, S. Shibata, Y. Yoshida, Z. Gu, A. Kimura, C. Ma, C. Xu, W. Bando, K. Fujita, K. Shinomiya, T. Hirai, Y. Asou, M. Enomoto, H. Okano, A. Okawa, H. Itoh, Nature **497**, 490–493 (2013). https://doi.org/10.1038/nature12115
15. S. Yoshida, N. Wada, D. Hasegawa, H. Miyaji, H. Mitarai, A. Tomokiyo, S. Hamano, H. Maeda J. Dental Res. **95**, 1282–1290 (2016). https://doi.org/10.1177/0022034516653085
16. Y. Akita, S. Kuroshima, K. Nakajima, H. Hayano, R. Kanai, M. Sasaki, T. Sawase, J. Bone Miner. Metab. **36**, 547–559 (2018). https://link.springer.com/article/10.1007/s00774-017-0872-1
17. N. Fedchenko, J. Reifenrath, Diagn. Pathol. **9**, 221 (2014). https://doi.org/10.1186/s13000-014-0221-9
18. T. Furihata, H. Miyaji, E. Nishida, A. Kato, S. Miyata, K. Shitomi, K. Mayumi, Y. Kanemoto, T.

Sugaya, T. Akasaka, J. Biomed. Mater. Res. B Appl. Biomater. **108**, 3033–3044 (2020). https://doi.org/10.1002/jbm.b.34632

19. A. Pal, A. Oyane, M. Nakamura, K. Koga, E. Nishida, H. Miyaji, Int. J. Mol. Sci. **25**, 1495 (2024). https://doi.org/10.3390/ijms25031495
20. L. Bacakova, K. Novotna, D. Hadraba, J, Musilkova, P. Slepicka, M. Beran, Polymers **14**, 602 (2022). https://doi.org/10.3390/polym14030602
21. X. Wang, A. Ito, Y. Sogo, X. Li, H. Tsurushima, A. Oyane, Acta Biomater. **5**, 2647–2656 (2009). https://doi.org/10.1016/j.actbio.2009.03.020
22. R. Lakra, M.S. Kiran, P.S. Korrapati, Int. J. Biol. Macromol. **166**, 333–341 (2021). https://doi.org/10.1016/j.ijbiomac.2020.10.193
23. E.M. Lotz, M.B. Berger, B.D. Boyan, Z. Schwartz, Bone **134**, 115260 (2020). https://doi.org/10.1016/j.bone.2020.115260
24. L. Liu, J. Wang, X. Song, Q. Zhu, S. Shen, W. Zhang, Exp. Ther. Med. **15**, 3489–3494 (2018). https://doi.org/10.3892/etm.2018.5813